

Effect of Magnetic Field Direction on Magnetoresistivity, Activation Energy, Irreversibility and Upper Critical Field of Bi-2212 Thin Film Fabricated by DC Sputtering Method

G. Yildirim · S. Bal · A. Varilci

Published online: 19 February 2012
© Springer Science+Business Media, LLC 2012

Abstract This study aims to investigate the effect of magnetic field direction on superconducting properties of Bi-2212 thin film fabricated on MgO (100) substrate using the direct current (DC) magnetron reactive sputtering technique at 100 watt with the aid of magnetoresistivity measurements. The zero resistivity transition temperatures (T_c), irreversibility fields ($\mu_0 H_{irr}$) and upper critical fields ($\mu_0 H_{c2}$) are deduced from the magnetoresistivity versus temperature curves under DC magnetic fields (parallel and perpendicular to c -axis) up to 5 T. Moreover, thermally activated flux flow (TAFF) model is studied for activation energy (U_0) values of the sample. It is found that the T_c value decreases from 76.4 K to 39.1 K for the applied magnetic field perpendicular to c -axis ($\mu_0 H \perp c$ -axis); likewise, the T_c reduces towards 28.8 K with the increase in the applied field parallel to c -axis ($\mu_0 H \parallel c$ -axis). Furthermore, the U_0 values are found to decrease considerably with increasing applied magnetic field. In fact, the U_0 of 134.5 K is obtained to be smallest at 5 T field parallel to the c -axis. Additionally, both the $\mu_0 H_{irr}$ and $\mu_0 H_{c2}$ values determined are also observed to reduce with the increase of the applied magnetic field. At absolute zero temperature ($T = 0$ K), the extrapolation of the $\mu_0 H_{irr}(T)$ and $\mu_0 H_{c2}(T)$ curves is used to obtain the $\mu_0 H_{irr}(0)$ and $\mu_0 H_{c2}(0)$ values of the film, respectively. The inner is found to be about 22.216 T (19.046 T) for the applied field perpendicular (parallel) to c -axis whereas the latter is determined to be about 54.095 T (126.522 T) for the applied field parallel (perpendicular) to c -axis, respectively, as a result of anisotropic behavior of the film prepared. On the other

hand, penetration depths (λ) and coherence lengths (ξ) inferred from $\mu_0 H_{irr}(0)$ and $\mu_0 H_{c2}(0)$ values are obtained to be about 38.519 Å (41.601 Å) and 16.147 Å (24.685 Å) in the case of applied field perpendicular (parallel) to c -axis, respectively. Based on all the results, the change of the superconducting properties as a function of the magnetic field direction presents the anisotropy of the sample produced. X-ray diffraction (XRD) and scanning electron microscopy (SEM) examinations are also conducted for microstructural and phase analyses of the film.

Keywords Bi-2212 thin film · Magnetoresistivity · TAFF model · Activation energy · Irreversibility field · Upper critical field

1 Introduction

As well known, the applications of the superconductor materials in high magnetic fields and temperatures are trouble for researchers during the discovery of the superconductivity. Therefore, the researchers have attempted to improve the superconducting, mechanical, structural and flux pinning properties of the superconductors to make them suitable for high temperature and magnetic field applications [1–4]. The Bi–Sr–Ca–Cu–O (BSSCO) materials, one of the cuprate high-temperature superconductor families, have widely been investigated because of their higher critical temperature, remarkable smaller power losses, higher current and magnetic field carrying capacity, optical and electronic properties [5–13]. Moreover, in the literature there have been several reports relating to BSSCO films for high frequency applications including filters, antennas and magnetic shield devices [14–17]. This family has three different phases with regard to chemical compositions: the Bi-2201 phase with T_c of ≈ 20 K, Bi-2212 phase with T_c of

G. Yildirim · S. Bal (✉) · A. Varilci
Department of Physics, Abant Izzet Baysal University,
Bolu 14280, Turkey
e-mail: sevgiibal@gmail.com

≈ 85 K and Bi-2223 phase with T_c of ≈ 110 K [18]. In these phases, Bi-2212 consisting of the double layered cuprate obtains more advantageous than the others in terms of the relatively invariant of the oxygen stoichiometry with respect to cationic doping, lesser weak link problems and better thermodynamic stability [19, 20]. On the other hand, the Bi-2212 thin films have the strong anisotropic property, very low charge carrier density, extremely short coherence length (ξ) and large penetration depth (λ), causing to limitation of its applications in high magnetic fields and temperatures. If the Bi-2212 film is exposed to high magnetic fields and temperatures, unusually rapid flux flow starts to appear in the sample, resulting in the energy dissipation and subsequent transition of superconductor to the normal state [21]. In order to overcome these problems appeared, the flux pinning mechanism in the film should be investigated in detail. In the recent works [12–24], the researchers have extensively analyzed the flux pinning mechanism in the superconducting state to introduce the effective pinning centers such as planar defects, stacking faults, and microdefects, resulting in thermally activated jumps; or hopping of flux lines; or flux bundles over an energy barrier [25, 26]. Over the pinning energy barrier of a structure, the flux line might be thermally activated although the Lorentz force exerted on the flux bundle by the current is smaller than the pinning force [27–30]. A model, described as thermally activated flux flow (TAFF), works well in the resistivity region near T_c as a result of the zero resistivity ($\rho = 0$) [31–34]. Additionally, the width of the superconducting transition depends strongly on the anisotropy associated with the magnetic field direction with regard to the Cu–O planes (the c -axis) in the structure [35–39]. Flux pinning ability can also be estimated from the flux pinning force density and activation energy values because, as well known, the activation energy (mentioned as the potential barrier height) is generally regarded as a measure of flux pinning strength of a superconductor material [40, 41]. The activation energy is inferred from TAFF theory described with Arrhenius equation [$\rho = \rho_0 \exp(-U_0/k_B T)$], which will be dealt with in detail in results and discussion part.

In this study, the role of magnetic field direction on the superconducting of the Bi-2212 thin film produced on MgO (100) substrate by means of the direct current sputtering technique at 100 watt is analyzed by the magnetoresistivity measurements. It is found that the critical transition temperature decreases with the increase in the applied magnetic field and the change of the applied field direction with regard to the c -axis. Additionally, thermally activated flux flow (TAFF) model is modified to fit the magnetoresistivity curves at different applied field strengths up to 5 T. The activation energy, irreversibility field and upper critical field values of the film are determined by the TAFF model. Based on the results, the superconducting properties of the Bi-2212

film are found to be strongly dependent on the magnetic field direction, confirming the presence of anisotropy in the film.

2 Experimental Details

Superconducting Bi-2212 thin film are produced by means of the DC magnetron reactive sputtering method at 100 watt. Target with the nominal stoichiometry of $\text{Bi}_{1.6}\text{Pb}_{0.5}\text{Sr}_2\text{Ca}_{1.1}\text{Cu}_{2.1}\text{O}_y$ are elaborated in air by a solid-state synthesis [42, 43] using high purity chemicals Bi_2O_3 , PbO , SrCO_3 , CaCO_3 and CuO powders (Alfa Aesar Co., Ltd. 99.99%). The accurately weighed ingredients are homogeneously mixed in a grinding machine for 12 hours and calcined at 800°C for 12 hours in a tube furnace (Protherm-Model PTF12/75/200) at 5°C per minute heating rate. The resultant powder is reground to improve the homogeneity of the target and pelletized into cylindrical bar of $25\text{ mm} \times 25\text{ mm} \times 5\text{ mm}$ at 260 MPa compaction pressure. The target prepared is exposed to the calcination process at 830°C for 12 h in the tube furnace and cooled down to room temperature in air atmosphere. Both the heating and cooling rates of the furnace are adjusted to be $5^\circ\text{C}/\text{min}$. Prior to coating, the MgO (100) single crystal substrate with dimensions of $10 \times 10 \times 5\text{ mm}^3$ is ultrasonically cleaned by acetone and rinsed thoroughly with deionized water and then dried by way of nitrogenous gas. Thus, both the target and crystal substrate are placed in the sputtering chamber. After the distance between the target and substrate is adjusted to be about 40 mm, the chamber is evacuated with the aid of rotary and turbo pump down to 4.75×10^{-6} bars, then 100 W DC power is applied between the target and plate. A film is deposited on the MgO substrate at 70°C for 3 hours. The sintering process of the film deposited is carried out at 840°C for 6 hours.

The electrical resistivity measurements from 20 until 100 K are conducted by means of conventional four-probe method. The current and potential leads of high-grade copper wires are connected to the samples with silver paint for minimization of the contact resistance, obtained by annealing silver paste at 200°C for 6 h on the surface of the samples. A Keithley 220 programmable current source and a Keithley 2182A nano-voltmeter are used for the resistivity measurements. Furthermore, the resistivity versus temperature measurements are performed at various magnetic fields such as 0, 0.5, 1, 3 and 5 T (parallel and perpendicular to c -axis) by means of a He gas contact cryocooler and superconducting coil magnet from CRYO Industries at constant driving current of 1 mA.

These measurements are automated using GPIB interfaced with a PC. All the data obtained are recorded via Labview computer software. The superconducting critical

temperature (T_c) values of the film prepared are also determined from the magnetoresistivity measurements. Additionally, the irreversibility field ($\mu_0 H_{irr}$) and upper critical field ($\mu_0 H_{c2}$) are estimated from the resistivity versus the applied magnetic field curves. As received at various magnetic fields the $\mu_0 H_{irr}(T)$ and $\mu_0 H_{c2}(T)$ are defined as the fields where the temperature-dependent resistance is $R(\mu_0 H_{irr}, T) = 0.1R_n$ and $R(\mu_0 H_{c2}, T) = 0.9R_n$ (normal state resistance), respectively [44–48]. The intercepts of extrapolation of $\mu_0 H_{irr}(T)$ and $\mu_0 H_{c2}(T)$ to zero on the temperature axis are taken as the direct $\mu_0 H_{irr}(0)$ and $\mu_0 H_{c2}(0)$, respectively [49]. Coherence length (ξ) and penetration depth (λ) values at the absolute zero temperature are obtained from the upper critical magnetic field and irreversibility field values, respectively. Moreover, activation energy values of the film are calculated using line pinning model and making linear fits to the low resistivity part of the transition [50–53].

Structural and phase analysis of the film prepared in this work are determined by X-ray diffractometer (XRD) analysis at room temperature (Rigaku multiflex diffractometer), using $CuK\alpha$ radiation with wavelength of 0.15418 nm and incident angles in the range of 2θ between 3° and 60° at a scan speed of $3^\circ/\text{min}$ and a step increment of 0.02° . The X-ray tube voltage and the current were 36 kV and 26 mA, respectively.

The microstructure of freshly fractured surface of the samples is investigated by a Jeol scanning electron microscope (JEOL 6390-LV) with an accelerating voltage of 20 kV in the secondary electron image mode.

3 Results and Discussion

3.1 Magnetoresistivity Measurements

The variation of the normalized resistivity versus temperature at different applied magnetic fields (0, 0.5, 1, 3, and 5 T) for the (Bi, Pb)-2212 films produced on MgO (100) substrate using the DC magnetron reactive sputtering technique at 100 watt is studied in the temperature range 20–100 K and the results observed are given in Fig. 1. It is visible from the figure that the superconducting film exhibits metallic behavior above critical transition temperature and the T_c value systematically reduces with the increase of the applied magnetic field (Table 1). Whereas T_c of the sample is observed to decrease from 76.4 K to 39.1 K under 5 T field applied perpendicular to c -axis ($\mu_0 H \perp c$ -axis), the T_c is noticed to reduce towards 28.8 K at 5 T field parallel to c -axis ($\mu_0 H \parallel c$ -axis), indicating the anisotropic character of the Bi-2212 film prepared in this work. Similar results were reported in the literature [54, 55]. Figure 1 also illustrates that the magnetic field mostly affects the intergranular coupling of

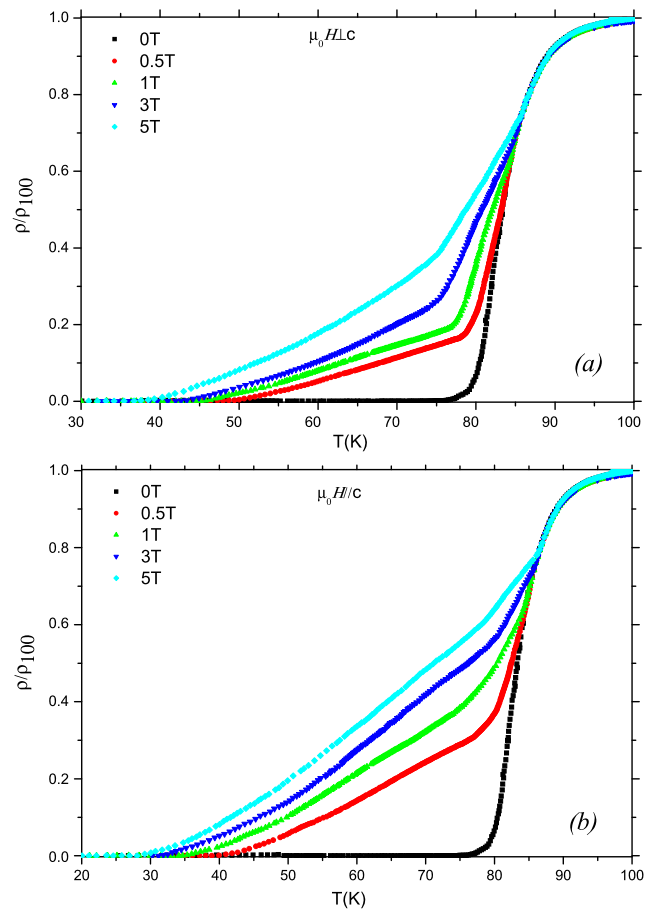


Fig. 1 Normalized magnetoresistivity ($\rho-T$) plots of the sample in applied magnetic fields (a) perpendicular and (b) parallel to c -axis up to 5 T

Table 1 Critical transition temperature (K) and activation energy (K) values of the sample under various applied field direction

Magnetic field	T_c (K)		$U(H)$ (K)	
	$\mu_0 H \perp c$	$\mu_0 H \parallel c$	$\mu_0 H \perp c$	$\mu_0 H \parallel c$
0 T	76.4	76.4	3906.4	3906.4
0.5 T	50.2	42.9	839.5	453.8
1 T	46.6	36.0	579.3	345.1
3 T	44.3	32.5	347.9	198.7
5 T	39.1	28.8	269.2	164.5

the sample produced. In other words, the onset critical temperature (T_c^{onset}) of the sample do not change significantly while the offset critical temperature (T_c) decrease dramatically with the applied magnetic field because of the fluxons motion [56]. Hence, the variation of $\Delta T_c (T_c^{\text{onset}} - T_c)$ is found to enhance with the increase of the applied magnetic field (especially parallel to c -axis) affecting drastically on the broadening of the resistive transition of the film. The maximum ΔT_c is observed to be about 49.1 K and 59.4 K

at 5 T applied field perpendicular and parallel to c -axis, respectively (Table 1), related to the increase of the flux pinning force in the sample [27, 28, 57]. In other words, the pinning ability of the sample in parallel field to the c -axis is found to be weaker than that in perpendicular to the c -axis.

3.2 Irreversibility and Upper Critical Field

The variation of the temperature as a function of the irreversibility field ($\mu_0 H_{irr}$) and upper critical field ($\mu_0 H_{c2}$) determined for the sample is shown in Fig. 2. It is apparent from the figure that the $\mu_0 H_{irr}$ and $\mu_0 H_{c2}$ curves of the sample not only increase with the decrease in the temperature but shift to lower temperatures as the applied magnetic field increases. The extrapolation of the curves at absolute zero temperature ($T = 0$ K) is used for the determination of the $\mu_0 H_{irr}(0)$ and $\mu_0 H_{c2}(0)$ values of the sample studied [58] so that we can easily calculate and discuss the coherence length (ξ) and penetration depth (λ) values which are from important parameters for superconductivity. The $\mu_0 H_{irr}(0)$ and $\mu_0 H_{c2}(0)$ values obtained are listed in Table 2. As seen from the table, the $\mu_0 H_{irr}(0)$ is observed to be about 22.216 T and 19.046 T at the applied field perpendicular and parallel to c -axis, respectively. The similar change is obtained for the $\mu_0 H_{c2}(0)$ value. Namely, the $\mu_0 H_{c2}(0)$ is found to be about 126.522 T and 54.095 T under the applied field perpendicular and parallel to c -axis, respectively (Table 2), confirming the decrease in the pinning ability because

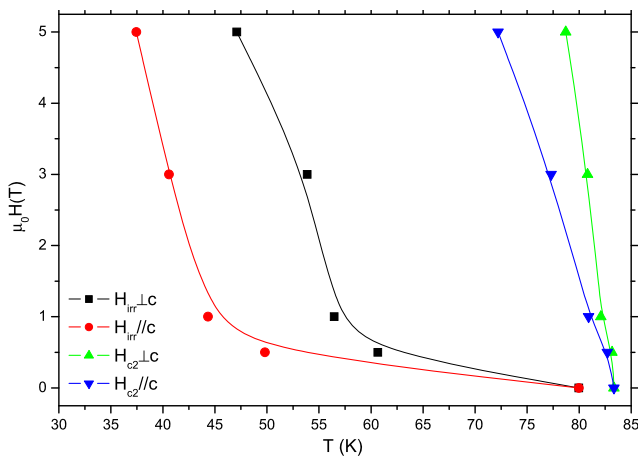


Fig. 2 Temperature dependences of the irreversibility field ($\mu_0 H_{irr}$) and upper critical field ($\mu_0 H_{c2}$) at several constant magnetic fields applied parallel and perpendicular to c -axis up to 5 T

of the anisotropic behavior of the Bi-2212 film produced. As for the coherence length and penetration depth values, it is well known the directly determination of these parameters is difficult task. However, the ξ and λ values at the absolute zero temperature can be calculated from the upper critical magnetic field and irreversibility field, respectively. The coherence length $\xi(0)$ and penetration depth $\lambda(0)$ at $T = 0$ K are defined as,

$$\xi(T) = \left[\frac{\phi_0}{2\pi \mu_0 H_{c2}(T)} \right]^{\frac{1}{2}} \quad \text{and} \quad (1)$$

$$\lambda(T) = \left[\frac{\phi_0}{2\pi \mu_0 H_{irr}(T)} \right]^{\frac{1}{2}}$$

where $\phi_0 = 2.07 \times 10^{-15} \text{ Tm}^2$. The $\xi(0)$ and $\lambda(0)$ values calculated from (1) are tabulated in Table 2. As seen from the table, the penetration depth value is obtained to be about 38.519 Å and 41.601 Å whereas the coherence length value is calculated to be about 16.147 Å and 24.685 Å under the applied field perpendicular and parallel to c -axis, respectively.

3.3 Activation Energy

Activation energy (U_0), playing an important role as the potential energy barrier to keep the magnetic flux in pinning center, is determined from the magnetoresistivity curves [39]. In a superconductor, when the pinning force is strong sufficiently, vortex motion can be appeared small enough in the material so that the superconductor acts as a perfect conductor. However, whenever the superconductor is subjected to the strong currents, there will always be thermally activated flux flow (TAFF) where vortices hop from one pinning site to an adjacent pinning site, and in some cases, the rate stemmed from transition of the vortices can be measured [59–61]. Moreover, TAFF is an essential dissipation mechanism causing to a long resistive tail for the temperatures below the superconducting transition temperature [62, 63]. Hence, the magnetoresistivity measurements give the reliable results for the activation energy values. In this study, the activation energies of the film are inferred from the line pinning model by making linear fits to the low resistivity part of the transition. Namely, the variation of logarithmic resistivity as a function of the reciprocal of temperature for the film at various applied magnetic fields such as 0, 0.5, 1, 3 and 5 T is plotted and the activation energies are estimated

Table 2 Irreversibility field, upper critical field, coherence length and penetration depth values of the sample at absolute zero temperature ($T = 0$)

$\mu_0 H \perp c$				$\mu_0 H \parallel c$			
$\mu_0 H_{c2}(0)$	$\mu_0 H_{irr}(0)$	$\lambda(0)$	$\xi(0)$	$\mu_0 H_{c2}(0)$	$\mu_0 H_{irr}(0)$	$\lambda(0)$	$\xi(0)$
126.522	22.216	38.5188	16.1471	54.095	19.046	41.601	24.685

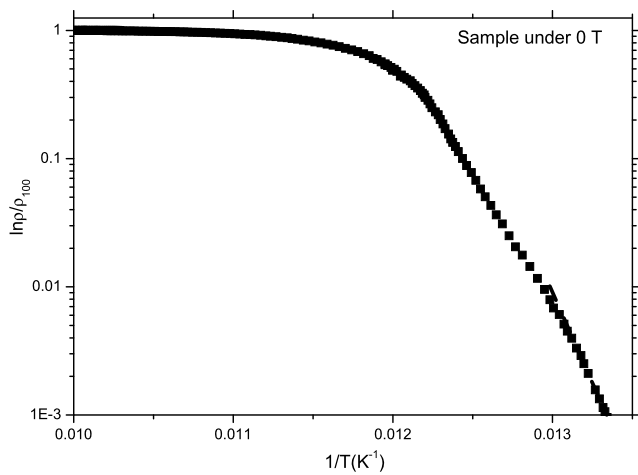


Fig. 3 The linear fit of the $\ln \rho / \rho_0$ versus $1/T$ graph for the sample without any magnetic field (the lines are guides for the eye)

from the slope of the linear part of the low resistivity region. Figure 3 shows that how we fit the $\ln \rho / \rho_0$ versus $1/T$ plot named as Arrhenius graph [64, 65]. As seen from the figure, the lines are guides for the eye and the slope of the straight line of the low resistivity region is assigned as the activation energy value. The Arrhenius plots of the magnetoresistivity data are depicted in Fig. 4. It is demonstrated from the figure that the energy dissipation (the resistivity) is due to the thermal activation of flux across the pinning barrier. The current-independent resistivity can be described by Arrhenius law, [66–69] $\rho = \rho_0 \exp(-U_0/k_B T)$, where U_0 is the activation energy, k_B is the universal Boltzmann’s constant and ρ_0 is a field-independent pre-exponential factor. For the sample, the activation energies calculated (in Kelvin unit) are given in Table 1. As seen from the table, the activation energy values decrease dramatically with the increase of the applied magnetic field to a minimum due to the decrement of the energy barriers in the sample produced in this work. The minimum U_0 value is found to be about 357.2 K (134.5 K) at the field applied perpendicular (parallel) to c -axis, associated with anisotropic behavior of the film. Furthermore, Table 1 indicates an important point that the activation energy values for both field directions reduce drastically up to 0.5 T and then decrease slightly because of the fact that the applied magnetic field penetrates only the intergranular media below that value.

Additionally, the field dependence of the activation energy of the samples is analyzed by means of the log–log plot of activation energy versus applied magnetic field (Fig. 5). The relation obtained from the figure is observed to be linear and the field dependence of the activation energy can also be described by a power law as

$$U(H) \propto H^{-\beta} \tag{2}$$

When the data obtained from the measurements are fitted to (2), the β values are found to be about 0.489 and 0.452

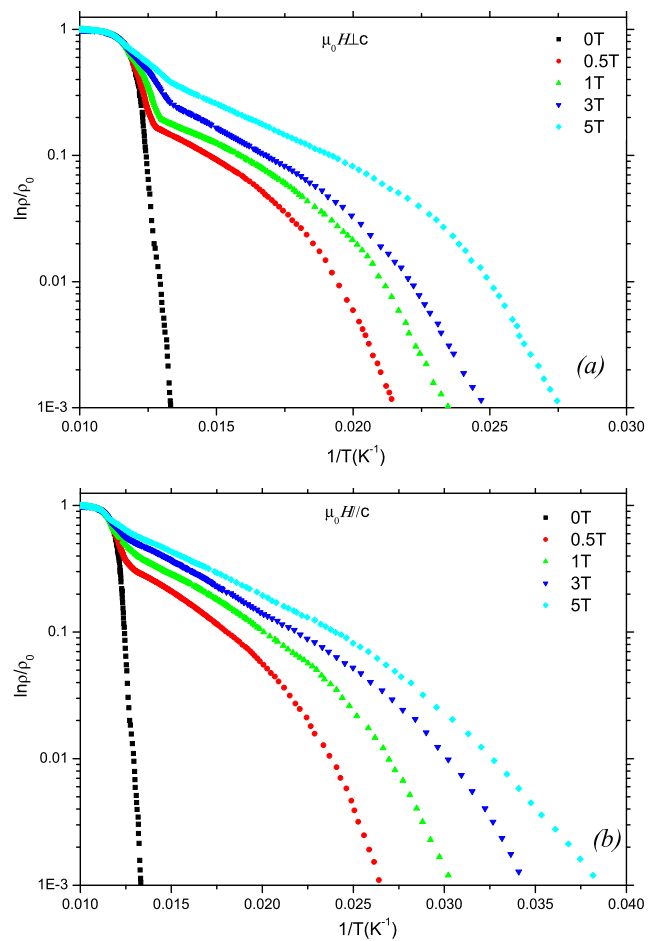


Fig. 4 $\ln \rho / \rho_0$ versus $1/T$ graphs of the sample (a) the field applied perpendicular to c -axis ($\mu_0 H \perp c$ -axis) and (b) the field applied parallel to c -axis ($\mu_0 H \parallel c$ -axis). The activation energies of the sample are determined from the slopes of the linear parts of the low resistivity region

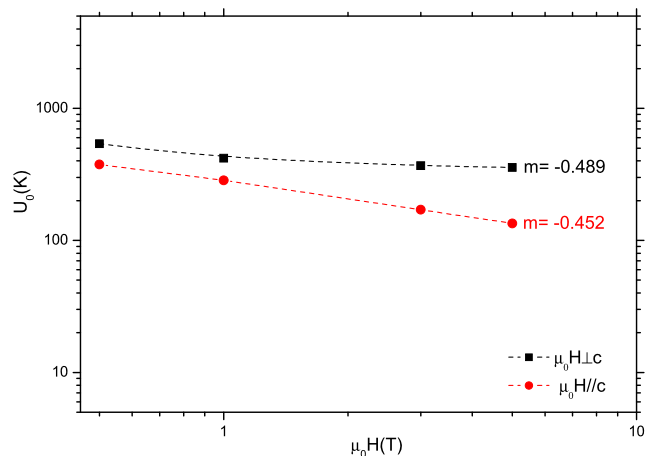


Fig. 5 Applied magnetic field dependence of activation energy U_0 for the film (the lines are guides for the eye)

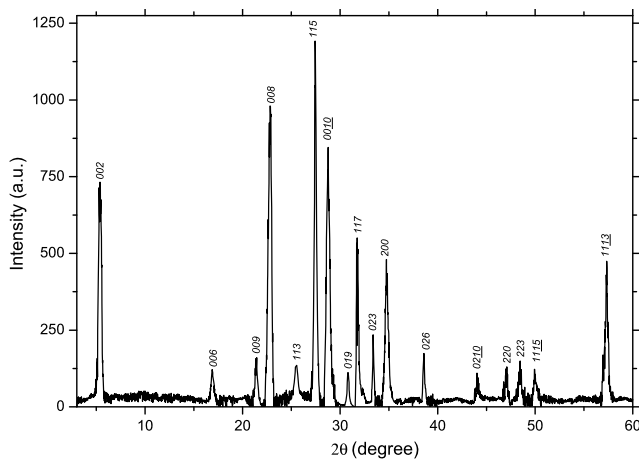


Fig. 6 XRD patterns of the sample

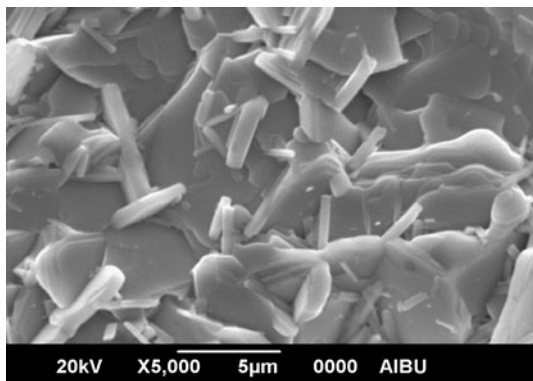


Fig. 7 SEM micrographs of the film produced

for the field applied perpendicular and parallel to c -axis, respectively. For $\beta = 0.5$, the activation energy is related to the plastic deformation of flux line lattice at dislocations, similar to the thermally activated motion of edge dislocations in crystals [70, 71]. In the recent works, the β was also found to be about 0.5 for the Bi-2212 and Bi-2223 phase [72, 73].

3.4 Microstructural and Phase Analyses

For phase and microstructural analyses of the film fabricated in this work, X-ray diffraction (XRD) and scanning electron microscopy (SEM) measurements are performed. Figure 6 indicates the XRD patterns between 3° and 60° for the sample. In the diagram, the corresponding (hkl) Miller indices result from Bi-2212 phase. The figure shows that the sample only exhibits the polycrystalline superconducting Bi-2212 phase. Moreover, ($00l$) peaks are dominant features for the film and the c -axes in the sample are oriented in the direction normal to the substrate surface, leading to the anisotropic character. Figure 7 illustrates the SEM image of the fractured surface of the sample. One can see from the figure, the sample has a fine crystalline homogeneous structure consisting of the clear and flaky grains with layered growth [74].

The surface of the sample is also found to be uniform with a well alignment of grains. Moreover, the grain boundaries are likely to have weak links, related to the decrement in the intergranular coupling, confirming that not only why the superconducting properties of the sample studied decrease with the increase in the applied magnetic field but why the sample exhibits the anisotropic behavior, as well.

4 Conclusion

In this study, it is examined that how the magnetic field direction affects the superconducting properties of Bi-2212 thin film produced by the direct current (DC) magnetron reactive sputtering technique with the aid of magnetoresistivity measurements. The important physical properties of the sample such as T_c , U_0 , $\mu_0 H_{irr}$, $\mu_0 H_{c2}$, λ and ξ values are inferred from the ρ - T curves under DC magnetic fields (parallel and perpendicular to c -axis) up to 5 T. The results indicate that these properties depend strongly on the magnetic field direction. The minimum T_c value is found to be about 39.1 K and 28.8 K under 5 T field perpendicular and parallel to c -axis, respectively. The similar trend is observed for activation energy value determined using thermally activated flux creep model. The minimum U_0 value is obtained to be about 357.2 K and 134.5 K at 5 T field applied perpendicular and parallel to c -axis. Furthermore, the change of the irreversibility field, upper critical field, penetration depth and coherence length values with regard to the magnetic field direction shows the anisotropic nature of the Bi-2212 film produced. As for the SEM investigation, the sample, the surface of which is found to be uniform with a well alignment of grains, obtains a fine crystalline homogeneous structure containing the clear and flaky grains with layered growth. Further, XRD results illustrate that in the Bi-2212 film produced, the ($00l$) peaks are dominant features and the c -axes are oriented in the direction normal to the substrate surface, leading to the anisotropic nature of the sample.

References

1. Sarun, P.M., Vinu, S., Shabna, R., Biju, A., Syamaprasad, U.: Mater. Res. Bull. **44**, 1017 (2009)
2. Terzioglu, C., Yilmazlar, M., Ozturk, O., Yanmaz, E.: Physica C **423**, 119 (2005)
3. Ozturk, O., Akdogan, M., Aydın, H., Yilmazlar, M., Terzioglu, C., Belenli, I.: Physica B **399**, 94 (2007)
4. Terzioglu, C., Ozturk, O., Kilic, A., Gencer, A., Belenli, I.: Physica C **434**, 153 (2006)
5. Yegen, D., Varilci, A., Yilmazlar, M., Terzioglu, C., Belenli, I.: Physica C **466**, 5 (2007)
6. Karaca, I., Celebi, S., Varilci, A., Malik, A.I.: Supercond. Sci. Technol. **16**, 100 (2003)
7. Varilci, A., Altunbas, M., Gorur, O., Karaca, I., Celebi, S.: Phys. Status Solidi A **194**, 206 (2002)

8. Mihalache, V., Aldica, G.: *J. Optoelectron. Adv. Mater.* **9**, 919 (2007)
9. Runde, M.: *IEEE Trans. Appl. Supercond.* **5**, 813 (1995)
10. Sedky, A.: *Physica C* **468**, 1041 (2008)
11. Okada, M.: *Sci. Technol.* **13**, 29 (2000)
12. Chanda, B., Dey, T.K.: *Magn. Supercond. Mater. A–B*, 295 (2000)
13. Asikuzun, E., Ozturk, O., Cetinkara, H.A., Yildirim, G., Varilci, A., Yilmazlar, M., Terzioglu, C.: *J. Mater. Sci. Mater. Electron* (2011). doi:[10.1007/s10854-011-0537-0](https://doi.org/10.1007/s10854-011-0537-0)
14. Phillips, J.M.: *J. Appl. Phys.* **79**, 1829 (1996)
15. Li, A.H., Ionescu, M., Wang, X.L., Dou, S.X., Wang, H.: *J. Alloys Compd.* **333**, 179 (2002)
16. Singh, R.K., Kumar, D.: *Mater. Sci. Eng.* **R22**, 113 (1998)
17. Alford, N.McN., Penn, S.J., Button, T.W.: *Supercond. Sci. Technol.* **10**, 169 (1997)
18. Ghahfarokhi, S.E.M., Shoushtari, M.Z.: *Physica B* **405**, 4643 (2010)
19. Miao, H., Meinesz, M., Czabai, B., Parrell, J., Hong, S.: *AIP Conf. Proc.* **986**, 423 (2008)
20. Biju, A., Aloysius, R.P., Syamaprasad, U.: *Supercond. Sci. Technol.* **18**, 1454 (2005)
21. Koyama, K., Kanno, S., Noguchi, S.: *Jpn. J. Appl. Phys.* **29**, L53 (1990)
22. Rentschler, T., Kemmlersack, S., Hartmann, M., Hubener, R.P., Kessler, P., Lichte, H.: *Physica C* **200**, 287 (1992)
23. Vinu, S., Sarun, P.M., Shabna, R., Biju, A., Syamaprasad, U.: *J. Appl. Phys.* **104**, 043905 (2008)
24. Wakata, M., Takano, S., Munakata, F., Yamauchi, H.: *Cryogenics* **32**, 1046 (1992)
25. Wan, X., Sun, Y., Song, W., Jiang, L., Wang, K., Du, J.: *Supercond. Sci. Technol.* **11**, 1079 (1998)
26. Vinu, S., Sarun, P.M., Shabna, R., Syamaprasad, U.: *J. Alloys Compd.* **487**, 1 (2009)
27. Tinkham, M.: *Introduction to Superconductivity*, 2nd edn. McGraw-Hill, New York (1996)
28. Sheahen, T.P.: *Introduction to High-Temperature Superconductivity*, 1st edn. Springer, New York (1994)
29. Yazici, D., Erdem, M., Ozcelik, B.: *J. Supercond. Nov. Magn.* (2011). doi:[10.1007/s10948-011-1331-1](https://doi.org/10.1007/s10948-011-1331-1)
30. Poole, C.P. Jr., Farach, R.J., Creswick, R.J., Prozorov, R.: *Superconductivity*, 2nd edn. Academic Press, London (2007)
31. Palstra, T.T., Batlogg, B., Schneemeyer, L.F., Waszczak, J.V.: *Phys. Rev. Lett.* **61**, 662 (1988)
32. Griessen, R.: *Phys. Rev. Lett.* **64**, 1674 (1990)
33. Malozemoff, A.P., Worthington, T.K., Zeldov, E., Yeh, N.C., McElfresh, M.W.: In: Fukuyama, H., Maekawa, S., Malozemoff, A.P. (eds.) *Strong Correlation and Superconductivity*. Springer Series in Sol. State Sci., vol. 89. Springer, Berlin (1989)
34. Ma, R.C., Song, W.H., Zhu, X.B., Zhang, L., Liu, S.M., Fang, J., Du, J.J., Sun, Y.P., Li, C.S., Yu, Z.M., Feng, Y., Zhang, P.X.: *Physica C* **405**, 34 (2004)
35. Charalambous, M., Chaussy, J., Lejay, P.: *Phys. Rev. B* **45**, 5091 (1992)
36. Dogruer, M., Zalaoglu, Y., Varilci, A., Terzioglu, C., Yildirim, G., Ozturk, O.: *J. Supercond. Nov. Magn.* (2011). doi:[10.1007/s10948-012-1403-x](https://doi.org/10.1007/s10948-012-1403-x)
37. Salem, A., Jakob, G., Adrian, H.: *Physica C* **402**, 354 (2004)
38. Xu, X.J., Fu, L., Wang, L.B., Zhang, Y.H., Fang, J., Cao, X.W., Li, K.B., Hisashi, S.: *Phys. Rev. B* **59**, 608 (1999)
39. Yildirim, G., Dogruer, M., Ozturk, O., Varilci, A., Terzioglu, C., Zalaoglu, Y.: *J. Supercond. Nov. Magn.* (2011). doi:[10.1007/s10948-011-1384-1](https://doi.org/10.1007/s10948-011-1384-1)
40. Pu, M.H., Song, W.H., Zhao, B., Wu, X.C., Sun, Y.P., Du, J.J., Fang, J.: *Physica C* **361**, 181 (2001)
41. Yildirim, G., Akdogan, M., Altintas, S.P., Erdem, M., Terzioglu, C., Varilci, A.: *Physica B* **406**, 2011 (1853)
42. Azzouz, B.F., Mchirgui, A., Yangui, B., Boulesteix, C., Salem, B.M.: *Physica C* **356**, 83 (2001)
43. Yildirim, G., Zalaoglu, Y., Akdogan, M., Altintas, S.P., Varilci, A., Terzioglu, C.: *J. Supercond. Nov. Magn.* **24**, 2153 (2011)
44. Moodera, J.S., Meservey, R., Tkaczyk, J.E., Hao, C.X., Gibson, G.A., Tedrow, P.M.: *Phys. Rev. B* **37**, 619 (1988)
45. Ososfky, M.S., Soulen, R.J., Wolf, S.A., Broto, J.M., Rakoto, J.M., Ousset, J.C., Coffe, G., Askenazy, S., Pari, P., Bozovic, I., Eckstein, J.N., Virshup, G.F.: *Phys. Rev. Lett.* **71**, 2315 (1993)
46. Erdem, M., Ozturk, O., Yucel, E., Altintas, S.P., Varilci, A., Terzioglu, C., Belenli, I.: *Physica B* **406**, 705 (2011)
47. Kitaguchi, H., Matsumoto, A., Hatakeyama, H., Kumakura, H.: *Supercond. Sci. Technol.* **17**, S486 (2004)
48. Kim, J.H., Dou, S.X., Shi, D.Q., Rindfleisch, M., Tomsic, M.: *Supercond. Sci. Technol.* **20**, 1026 (2007)
49. Yadav, C.S., Paulose, P.L.: *New J. Phys.* **11**, 103046 (2009)
50. Smith, G.B., Bell, J.M., Filipczuk, S.W., Andrikidis, C.: *Physica C* **160**, 333 (1989)
51. Vo, N.V., Liu, H.K., Dou, S.X.: *Supercond. Sci. Technol.* **9**, 104 (1996)
52. Inui, M., Littlewood, P.B., Coppersmith, S.N.: *Phys. Rev. Lett.* **63**, 2421 (1989)
53. Aksan, M.A., Yakinci, M.E., Guldeste, A.: *Thin Solid Films* **515**, 8022 (2007)
54. Martinez, H., Marino, A., Rodriguez, J.E.: *Physica C* **408–410**, 568 (2004)
55. Awana, V.P.S., Menon, L., Malik, S.K.: *Phys. Rev. B* **53**, 2245 (1996)
56. Yildirim, G., Bal, S., Yucel, E., Dogruer, M., Akdogan, M., Varilci, A., Terzioglu, C.: *J. Supercond. Nov. Magn.* (2011). doi:[10.1007/s10948-011-1324-0](https://doi.org/10.1007/s10948-011-1324-0)
57. Ozkurt, B., Ozcelik, B.: *J. Low Temp. Phys.* **156**, 22 (2009)
58. Yadav, C.S., Paulose, P.L.: *New J. Phys.* **11**, 103046 (2009)
59. Wang, Y., Wen, H.H.: *Europhys. Lett.* **81**, 57007 (2008)
60. Olson, C.J., Reichhardt, C., Nori, F.: *Phys. Rev. B* **56**, 6175 (1997)
61. Chen, X.J., Struzhkin, V., Wu, Z., Lin, H.Q., Hemley, R.J., Mao, H.K.: *Proc. Natl. Acad. Sci. USA* **104**, 3732 (2007)
62. Kusevic, I., Babic, E., Marohnic, Z., Ivkov, J., Liu, H.K., Dou, S.X.: *Physica C* **235–240**, 3035 (1993)
63. Liu, H.K., Guo, Y.C., Dou, S.X., Cassidy, S.M., Cohen, L., Perkins, G.K., Caplin, A.D.: *Physica C* **213**, 95 (1993)
64. Kucera, J.T., Orlando, T.P., Virshup, G., Eckstein, J.N.: *Phys. Rev. B* **46**, 11004 (1992)
65. Yamasaki, H., Endo, K., Kosaka, S., Umeda, M., Yoshida, S., Kajimura, K.: *Phys. Rev. Lett.* **70**, 3331 (1993)
66. Abou-Aly, A.I., Mostafa, M.F., Ibrahim, I.H., Awad, R., Al-Hajji, M.A.: *Supercond. Sci. Technol.* **15**, 938 (2002)
67. Sung, H.H., Yang, H.C., Chen, H.C., Horng, H.E., Yao, B.C.: *Chin. J. Phys.* **30**, 247 (1992)
68. Passos, C.A.C., Orlando, M.T.D., Fernandes, A.A.R., Oliveira, F.D.C., Simonetti, D.S.L., Fardin, J.F., Belich, H. Jr., Ferreira, M.M. Jr.: *Physica C* **419**, 25 (2005)
69. Pu, M.H., Feng, Y., Zhang, P.X., Wang, J.X., Du, J.J., Zhou, L.: *Physica C* **412–414**, 467 (2004)
70. Paradhan, A.K., Muralidhar, M., Feng, Y., Murakami, M., Nakao, K., Koshizuka, N.: *Phys. Rev. B* **64**, 172505 (2001)
71. Geshkenbein, V., Larkin, A., Feigelman, M., Vinokur, V.: *Physica C* **162–164**, 239 (1989)
72. Noetzel, R., Westerholt, K.: *Phys. Rev. B* **58**, 15108 (1998)
73. Soulen, R.J. Jr., Wolf, S.A.: *Physica C* **1–2**, 95 (1990)
74. Moodera, J.S., Meservey, R., Tkaczyk, J.E., Hao, C.X., Gibson, G.A., Tedrow, P.M.: *Phys. Rev. B* **37**, 619 (1988)